SOUND GENERATION MECHANISM IN TURBULENT MIXING LAYER

Gyung-Min Choi
CFD Technology Center,
National Aerospace Laboratory
Jindaiji-Higashi, Chofu, Tokyo 182-8522, Japan
choigm@nal.go.jp

Ye Li
Mazda Motor Corporation
Shinchi, Fucyumachi, Aki, Hiroshima 730-8670, Japan
liyege@muse.ocn.ne.jp

Mamoru Tanahashi, Toshio Miyauchi
Department of Mechanical and Aerospace Engineering,
Tokyo Institute of Technology
Ookayama, Meguro-ku, Tokyo 152-8552, Japan
mtanahas@mes.titech.ac.jp, tmiyauch@mes.titech.ac.jp

ABSTRACT

Direct numerical simulation (DNS) has been performed to clarify the mechanism of sound generation in three-dimensional turbulent mixing layer. The amplitude of pressure fluctuation increases dramatically in the period of vortex pairing, and the sound wave is radiated from the mixing layer. In contribution of acoustic source components in Lightlill's acoustic analogy, the magnitude of entropy component becomes comparable to that of Reynolds stress, while the Reynolds stress component is a major factor which dominates total acoustic source in the two-dimensional calculation. The roles of coherent fine scale structures on sound generation are investigated. The structure of Reynolds stress component is identical to that of coherent fine scale eddies even in the core region where large number of coherent fine scale structures appears. On the other hand, the entropy component shows sheet-like structure around coherent fine scale eddies, and is dominated by the energy dissipation rate. In addition, the far-field sound was predicted using acoustic analogies and compared with the DNS result. For the case of source size of 4Λ, where Λ is the most unstable wavelength, Lighthill's analogy can predict far-field sound excellently, however, the amplitude of pressure fluctuation predicted by Powell's analogy shows significantly large values compared with the DNS result. For the case of source size of 3Λ, while the pressure fluctuation predicted by Lighthill's analogy shows agreement with the DNS result before the period of vortex pairing, it shows slightly small value compared with the DNS result after the mixing transition.

INTRODUCTION

The study of sound generation in turbulent flow has received considerable interest in the last decades, because how to reduce the noise generated in various flow fields, such as gas turbine, jet engine and burner etc, becomes a serious issue in the industry society. Most of the noise is radiated from the high Reynolds number (Re) flow and it may cause many mechanical vibration or flame instabilities in the combustor.

The researches on sound generation usually can be divided into three groups, that is, acoustic analogy, experimental approaches and numerical simulation. As for acoustic analogy, many choices of acoustic source are possible, and simple formulations have been proposed by Lighthill(1952), Powell(1964) and Howe(1975), etc. The sources suggested by Lighthill and Powell-Howe have been evaluated by Crighton(1981) and the Powell-Howe's source has been transformed using nonlinear Helmholts vortex laws as well as Green's function (Möhring, 1978). In addition, a convected wave equation was derived, which are mainly applied to deal with the high Mach number flow (Phillips, 1960).

As for experimental approach clarifying the mechanism of sound generation, it is very difficult to measure the sound wave precisely in the far-field, because the pressure fluctuation in an acoustic far field is significantly small compared with that in the near field. Consequently, only a few experiments have been conducted to investigate the sound generation in turbulent flow. Laufer and Yen(1983) have studied the noise generation in a low Mach number jet experimentally. They investigated the relation between the sound source and the pairing of large-scale structures, and showed that the intensity of sound radiation varies nonlinearly with the source strength.

With the recent development of high-speed and large storage computer, analysis of the sound generation by DNS has been conducted. Sound radiation in the two-dimensional compressible mixing layer has been investigated by Ho et al.(1988) and the scattering of sound wave by a vortex was also investigated numerically and analytically by Colonius et al.(1994). As a step towards direct computation of sound generation in free shear flows, computation of far-field sound from compressible co-rotating vortices has been conducted and the results were compared with the prediction obtained by acoustic analogies (Mitchell et al., 1995). Sound generation in a two-dimensional spatially-developing mixing layer was investigated by using the numerical methods validated in model problem (Colonius et al., 1997). In addition to

DNS approach, large eddy simulation(LES) has been conducted to predict jet noise (Bastin et al., 1997), in which approach was based on Lighthill's analogy, together with a semi-deterministic modeling of turbulence (SDM).

The recent studies (Tanahashi et al., 1997a, 1997b) have revealed the existence of coherent fine scale eddies in turbulence. The coherent fine scale eddies show strong swirling motion which is characterized by velocity difference of the order of the turbulent intensity within the diameter of eight times of the Kolmogorov microscale. In the free shear flows such as mixing layers, the large scale structures are composed of huge number of the coherent fine scale eddies after the mixing transition and these fine scale eddies are expected to have important roles in the sound generation in turbulence. Because most of the past researches by direct numerical simulation (DNS) have been restricted to the two-dimensional flow field, it was impossible to investigate the effects of coherent fine scale eddies on the sound generation.

Therefore, DNS of temporally developing three-dimensional turbulent mixing layer is performed to clarify the mechanism of sound generation after mixing transition and the relation between coherent fine scale eddies and sound generation. In addition, the far-field sound is predicted using acoustic analogies, and the availability of Lighthill's and Powell's acoustic analogy is evaluated by comparing with the result of DNS.

DIRECT NUMERICAL SIMULATION OF COMPRESSIBLE MIXING LAYER

The external forces and bulk viscosity are assumed to be negligible in this work. The flow field is governed by the following mass, momentum and energy conservation equations and the equation of the state.

$$\frac{\partial \rho}{\partial t} + \frac{\partial (\rho u_j)}{\partial x_j} \tag{1}$$

$$\frac{\partial (\rho u_i)}{\partial t} + \frac{\partial (\rho u_i u_j)}{\partial x_j} + \frac{1}{\gamma M^2}\frac{\partial \rho}{\partial x_i} = \frac{1}{Re}\frac{\partial \tau_{ij}}{\partial x_j} \tag{2}$$

$$\frac{\partial (\rho T)}{\partial t} + \frac{\partial (\rho T u_j)}{\partial x_j} = \frac{\gamma}{PrRe}\frac{\partial}{\partial x_j}\left(\frac{\partial T}{\partial x_j}\right) - (\gamma - 1)p\frac{\partial u_j}{\partial x_j} + \frac{\gamma(\gamma-1)M^2}{Re}\tau_{ij}\frac{\partial u_i}{\partial x_j} \tag{3}$$

$$p = \rho T \tag{4}$$

where, x_i is the Cartesian coordinates(x,y,z), t is the time, u_i is the velocity components(u,v,w), ρ is the density, p is the pressure, T is the temperature, γ is the ratio of heat capacity and τ_{ij} is the viscous stress tensor defined by

$$\tau_{ij} = \frac{\partial u_i}{\partial x_j} + \frac{\partial u_j}{\partial x_i} - \frac{2}{3}\delta_{ij}\frac{\partial u_k}{\partial x_k} \tag{5}$$

The non-dimensional parameters Re, Pr and M in the above governing equations represent Reynolds number$(\Delta U_0 \delta_{\omega 0}/(\mu/\rho_0))$, Prandtl number$(C_p\mu/\lambda)$ and Mach number$(\Delta U_0/c_0)$, respectively, where ΔU_0 is the velocity difference, $\delta_{\omega 0}(\Delta U_0/(\partial U/\partial y)_{max})$ is initial vorticity thickness, μ is the viscosity, λ is the thermal conductivity, c_0 is the sound speed and C_p is the heat capacity at constant pressure. Here, the governing equations are non-dimensionalized by the density and temperature of the free-stream, the difference of free-stream velocities and the initial vorticity thickness. In this study, temporally developing mixing layer is simulated by DNS. Periodic boundary conditions are applied in the streamwise (x) and spanwise (z) directions, and non-reflecting boundary conditions (NSCBC) (Poinsot and Lele, 1992) are used in the transverse (y) direction. The governing equations are discretized by the spectral method in the x and z direction, and by the fourth-order central finite difference scheme in the y direction. Aliasing errors from nonlinear terms are fully removed by 3/2 rule in the x and z direction. A third-order low storage Runge-Kutta scheme is used to advance the governing equations in time. The computational domain in the x, y and z direction is selected to be 2Λ, 6Λ and $4/3\Lambda$ respectively, where Λ is the most unstable wavelength for the initial mean velocity profile. The simulation is performed on the mesh of $120\times1921\times80$ for the case of Re=600, Mc=0.2, Pr=0.7 and γ=1.4. Here, Mc represents the convective Mach number (Papamoschou and Roshko, 1988). The uniform grid points are used and the grid spacing are Δx=Δz=0.118, Δy=0.022. The time step is Δt=0.003 and the CFL number at the initial stage is 0.41. The initial velocity field is composed of a mean streamwise velocity and three-dimensional perturbations. The initial velocity field is composed of a hyperbolic tangent streamwise velocity and three-dimensional random perturbations that include the banded white noise (Tanahashi et al., 2001).

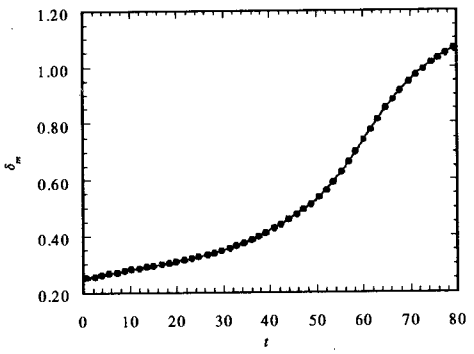

Figure 1: Development of momentum thickness

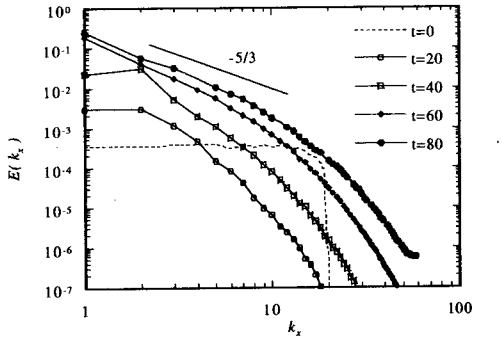

Figure 2: One-dimensional energy spectrum in the streamwise direction

STRUCTURE OF TURBULENT MIXING LAYER

In the mixing layer, the development of momentum thickness corresponds to the development of large-scale structure (Tanahashi and Miyauchi, 1993). Figure 1 shows the development of momentum thickness, which is averaged in the x-z plane. In the present study, the growth rate of momentum thickness increases dramatically in the period of pairing, while it is nearly constant in the process of vortex

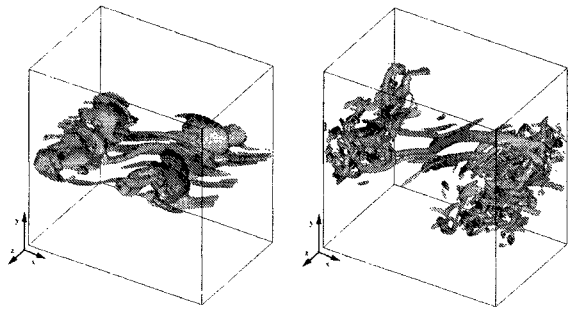

(a) t=40 (Q=0.03) (b) t=80 (Q=0.2)

Figure 3: Contour surfaces of the second invariant (Q) of velocity gradient tensor

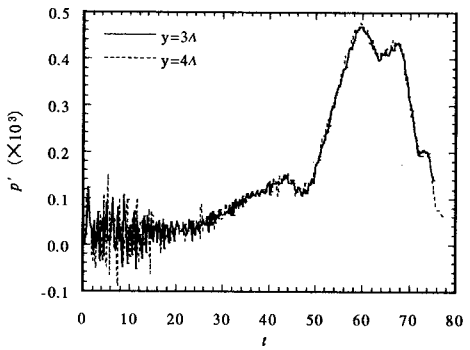

Figure 4: Temporal evolution of pressure fluctuations in the far field

roll-up (t <30). The momentum thickness reaches about 4 times of the initial value at the final stage of DNS in the present computation.

Figure 2 shows the one-dimensional energy spectrum in the streamwise direction. At a time of 40, the energy spectrum in the streamwise direction shows a peak at k_x=2. This indicates that two large-scale spanwise vortices are formed due to Kelvin-Helmholtz instability. In the late period of vortex pairing (t=80), the region where energy spectrum shows -5/3 power law is observed, which indicates that the mixing layer reaches fully developed state. These results agree with the observations in the experiments of turbulent mixing layer (Ho and Huerre, 1984, Huang and Ho, 1990).

It has been reported that the coherent fine scale structure of turbulence is well represented by the positive second invarient region in turbulence(Tanahashi et al., 1997a, 1997b). Figure 3 shows the contour surfaces of the second invarient of velocity gradient tensor. In the process of vortex roll-up(t=40), the streanwise eddies (rib structure) appear in the braid region, while no fine scale eddy is observed in the core region of large-scale structures. On the other hand, in the period of pairing(t=80), large number of fine scale eddies are observed in the core region. The appearance of these fine scale eddies indicates the occurrence of transition to turbulence(Tanahashi et al., 1997a)

MECHANISM OF SOUND GENERATION IN COMPRESSIBLE TURBULENT MIXING LAYER

Figure 4 shows the temporal evolution of pressure fluctuations in the far field. The measurement points are located at 3Λ and 4Λ in the transverse direction from the center of shear layer. In this figure, the time coordinate is shifted to adjust the sound propagating from the center to the measuring point. The initial pressure fluctuation (t <15) is ascribed to the three dimensional random perturbations of initial condition. The pressure fluctuation grows up gradually in the process of vortex roll-up (t <45), and it increases abruptly in the period of paring (50< t <65). In the process of the turbulence transition (65< t <70), the amplitude of pressure fluctuations keeps constant, then decreases significantly after the turbulence transition (t >70). It demonstrates that the amplitude of pressure fluctuation increases dramatically in turbulence transition of the turbulent mixing layer. Moreover, both the shape and amplitude of the pressure fluctuations are nearly identical (but shifted in time by Λ/c_0) at different planes (y=3Λ and 4Λ) in the acoustic far field. This result shows that the sound waves travel with the sound speed and the spurious numerical dispersion is insignificant.

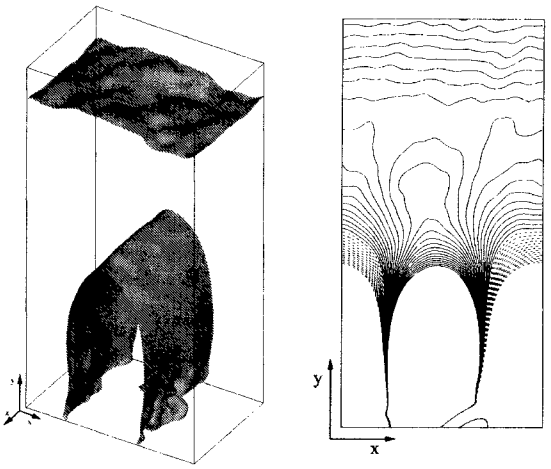

(a) $p\prime$=2.6 ×10^{-4} (b) $\Delta p\prime$=2 ×10^{-5}

Figure 5: Contour surfaces(a) and coutour lines(b) of pressure fluctuation at t=80

To investigate the characteristics of pressure fluctuation in detail, the contour surface and contour lines of pressure fluctuation at t=80 are shown in Fig.5. The contour surface near the center of mixing layer shows the pressure fluctuation in the near-field, while the contour surface near the boundary indicates the sound wave in the far-field. After the occurrence of turbulence transition, it shows that sound wave is radiated from the mixing layer. Moreover, from the shape of pressure fluctuation in the acoustic field, it can be seen that the sound wave can be approximated as one-dimensional plane wave propagating in the transverse direction. Furthermore, the contour plots of pressure fluctuation in the far-field show that the plane wave travels in the transverse direction without changing the shape. This indicates that the computational size used in the y direction is enough to capture the characteristics of the far-field sound wave.

As an acoustic analogy, Lighthill(1952) has rearranged the exact continuity and momentum equations into a wave equation with a source term on the right-hand side as follow:

$$\frac{\partial^2(\rho\prime)}{\partial t^2} - \frac{1}{M^2}\frac{\partial^2(\rho\prime)}{\partial x_i \partial x_i} = \frac{\partial^2 T_{ij}}{\partial x_i \partial x_j} \qquad (6)$$

where T_{ij} is the Lighthill's turbulent stress tensor defined by

$$T_{ij} = \rho u_i u_j + \frac{1}{M^2}\delta_{ij}\left(\frac{1}{\gamma}p - \rho\right) - \frac{1}{Re}\tau_{ij} \qquad (7)$$

In the present study, the total acoustic source term (T) is decomposed into three parts, as shown on the right hand side

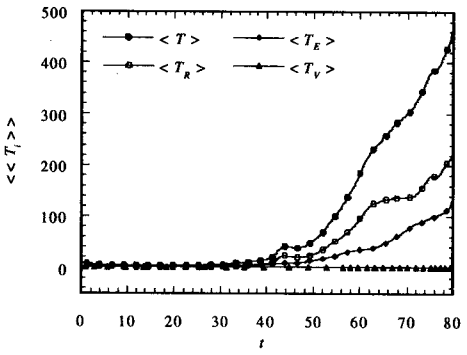

Figure 6: Contributions of each acoustic source term in Lighthill's acoustic analogy

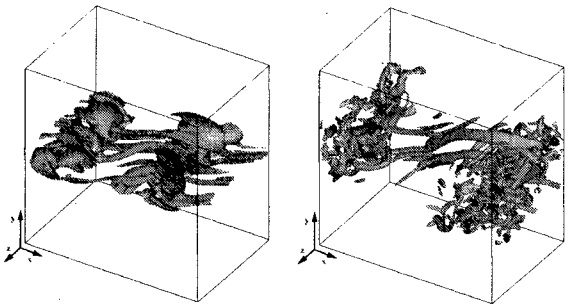

(a) t=40 (T_R=-0.06) (b) t=80 (T_R=-0.4)

Figure 7: Contour surfaces of Reynolds stress component (T_R) of acoustic source terms

of Eq. 7,: Reynolds stress (T_R), entropy (T_E) and viscous component (T_V), respectively.

Figure 6 shows the contributions of each acoustic source term in Lighthill's acoustic analogy. Though the total acoustic source term shows very small in the process of vortex roll-up, it increases significantly in the period of pairing. The figure shows that the contribution is in the order of $T_R > T_E > T_V$. The magnitude of T_E shows nearly the same order as T_R, while it is quite smaller than the T_R in the case of two-dimensional mixing layer without heat release(Li et al., 2000a). This will be discussed later.

Figure 7 shows the contour surfaces of Reynolds stress component of acoustic source terms. In the process of vortex roll-up(t=40), although some rib structures(streamwise vortex) appear in the braid region, no fine scale structure is observed in the core region. With the occurrence of mixing transition, Reynolds stress component becomes very complicated. After mixing transition (t=80), large number of of fine scale structures are observed in the core region even though the rib structure still exist in the braid region. The contour increment of Reynolds stress component is selected to be twice of the second invariant according to the relation of T_R=-2Q in the limitation of incompressible flow. It can be seen that the structure of Reynolds stress component is identical to the distribution of the second invarient even in the core region where large number of coherent fine scale structure appear. To investigate the relation between Reynolds stress component and the second invarient in detail, the contour plots of Reynolds stress component and the second invarient in the same x-y plane are shown in Fig. 8. At t=80, although large number of fine scale eddies appear resulting from mixing transition, the distribution of Reynolds stress component shows good agreement with that of the second invarient. This shows that the compressibility effect is weak, which is ascribed to low Mach number (M_c=0.2) in the present study. These results indicate that the mechanism of sound generation and coherent fine scale eddies can be related by means of the Reynolds stress component in turbulent mixing layer.

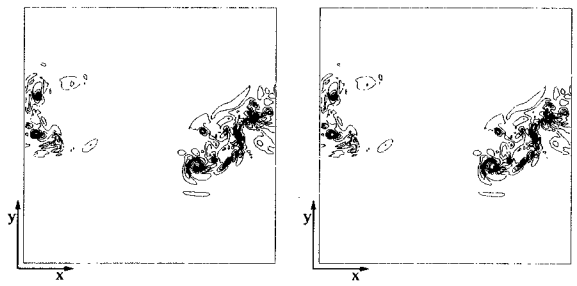

(a) ΔT_R=-0.4 (b) Q=0.2

Figure 8: Contour plots of Reynolds stress component and the second invarient in the same x-y plane(z=0), t=80

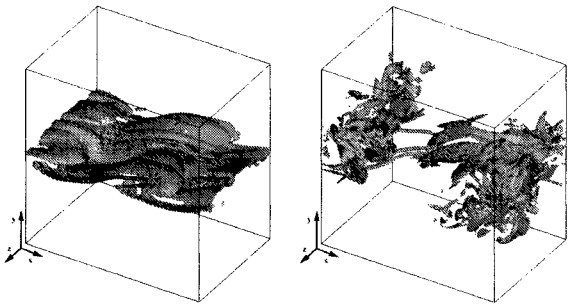

(a) t=40 (T_E=-0.08) (b) t=80 (T_E=-0.6)

Figure 9: Contour surfaces of entropy component in the Lighthill's acoustic analogy

Figure 9 shows the contour surfaces of entropy component of acoustic source terms. In the process of vortex roll-up (t=40), the entropy component shows sheet-like structure around large scales spanwise vortices. This sheet-like structure can be observed after the turbulence transition (t=80), even in the core region where large number of fine scale eddies exist.

To investigate the relation among the entropy component, coherent fine scale eddies and energy dissipation rate (ε), Fig. 10 shows contour plots of entropy component and distributions of the second invariant and energy dissipation rate at t=80. Because the coherent fine scale structures are represented by positive second invariant, only the distributions of positive second invariant are shown in these figures. Although the distributions of entropy component and the second invariant are very complicated, it is evident that the entropy component shows sheet-like structure around coherent fine scale eddies. It can be concluded that the coherent fine scale eddies play quite important role in the sound generation in turbulence. It has been reported that energy dissipation rate is distributed around coherent fine scale eddies in homogeneous isotropic turbulence (Tanahashi et al., 2000a) and incompressible turbulent mixing layers (Tanahashi et al., 1997a). The energy dissipation rate plays an important role in the sound generation in turbulence (Proudman, 1952, Lilley, 1994). From the figure of entropy component and energy dissipation rate, it is evident that the distribution of entropy component is quite similar to that of energy dissipation rate. Nearly same order of entropy component and Reynolds stress component shown in Fig. 6 can be attributed to this effect.

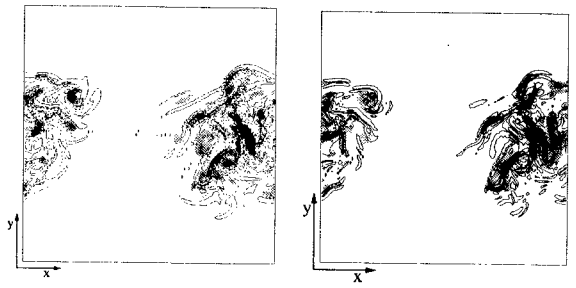

(a) T_E & Q (b) T_E & ε

Figure 10: Contour plots of entropy component and distributions of the second invariant and energy dissipation rate; line: entropy component, gray: the second invariant (a) and energy dissipation rate(ε) (b), t=80, $z = \Lambda$

PREDICTION OF FAR-FIELD SOUND USING ACOUSTIC ANALOGIES

Lighthill's (1952) and Powell's (1964) acoustic analogies are also evaluated by comparing the far-field sound predicted by acoustic analogies with the DNS results. In the prediction, the wave equations are discretized by the spectral method in the x and z direction and fourth-order central finite difference scheme in the y direction. A second-order Adams-Bashforth scheme is used to advance the wave equations in time. Periodic boundary condition is applied in the x and z direction and non-reflecting boundary conditions proposed by Engquist and Majda(1979) are used in the y direction. The computational grids and time step are same as those used in the DNS. When the wave equations are used to predict the far-field sound, the size of acoustic source used in the prediction is an important parameter (Li et al., 2000b). In the near field, the wave equations with the acoustic source term obtained by the DNS are solved. On the other hand, the wave equations, which express the propagation of sound wave, are solved without acoustic source in the far field. The source size is defined as the length of near-field in the y direction. Figure 11 shows the far-field pressure fluctuations predicted by Lighthill's and Powell's acoustic analogy. The DNS result is also plotted for comparison. Here, the source size is selected to be 4Λ. The far-field pressure fluctuation predicted by Lighthill's acoustic analogy shows good agreement with the DNS result, although the predicted pressure fluctuation contain some high frequency waves in the whole period. Compared with this, the amplitude of far-field pressure fluctuation predicted by Powell's acoustic analogy shows significantly larger value than the DNS result. This result indicates that Powell's acoustic analogy can not predict far-field sound correctly in turbulent mixing layer.

The contributions of Reynolds stress component and entropy components to the far-field sound predicted by Lighthill's acoustic analogy were also investigated and shown in Fig. 12. It can be seen that the pressure fluctuation predicted by Reynolds stress component is dominant on the whole, while the contribution by entropy component can not be neglected, especially in the period after mixing transition (t >65). Moreover, no high frequency wave was observed in the far-field sound predicted by entropy component, although high frequency wave corresponding to DNS is observed in that by Reynolds stress component. It could be seen that the high frequency wave predicted by Lighthill's acoustic analogy is ascribed to the Reynolds stress component.

The effect of source size on the predicted far-field sound will be explained. Figure 13 shows the far-field sound ob-

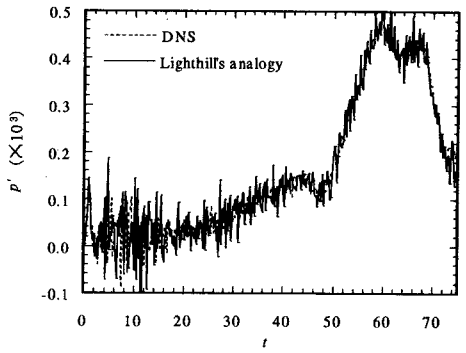

(a) Lighthill's acoustic analogy

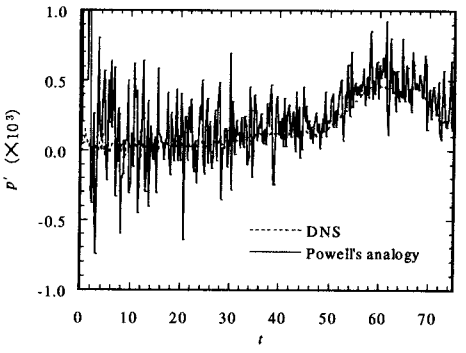

(b) Powell's acoustic analogy

Figure 11: Comparison of far-field sound obtained by DNS, and predicted by Lighthill's (a) and Powell's (b) acoustic analogy, source size: 4Λ

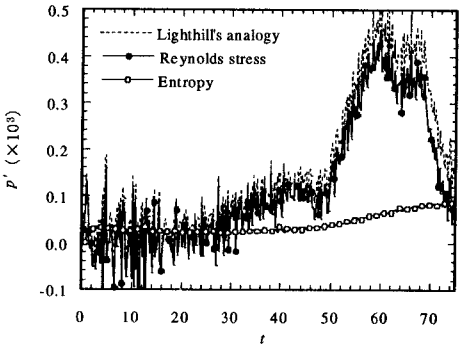

Figure 12: Contributions of Reynolds stress and entropy component on the far-field sound predicted by Lighthill's acoustic analogy, source size: 4Λ

tained by DNS and predicted by Lighthill's acoustic analogy, of which source size is 3Λ to compare with the result of Fig.11. The far-field pressure fluctuation predicted by Lighthill's acoustic analogy agrees with the DNS result until the period of vortex pairing(t <60). However, after the mixing transition, the amplitude of predicted pressure fluctuation show slightly small value compared with the DNS result. It implies that the source size of 3Λ is not enough to represent the Lighthill's acoustic source in this case.

SUMMARY

In this study, DNS has been conducted to clarify the mechanism of sound generation in three-dimensional turbulent mixing layer. The amplitude of pressure fluctuation increases dramatically in the process of vortex pairing, while it shows relatively low value in the vortex roll-up process. Af-

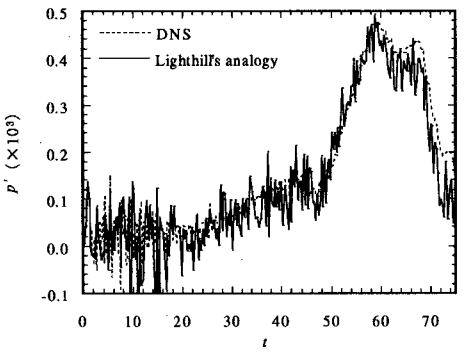

Figure 13: Comparison of far-field sound obtained by DNS and predicted by Lighthill's acoustic analogy, source size: 3Λ

ter the mixing transition, the pressure fluctuation decreases abruptly. The contribution of acoustic source components in Lightlill's acoustic analogy is relatively small in the process of vortex roll-up, and increases significantly in the period of pairing. The magnitude of entropy shows nearly same order as Reynolds stress component, and the entropy component is dominated by the energy dissipation rate.

The roles of coherent fine scale structures on sound generation are made clear by the DNS results. There exists a linear relation between the Reynolds stress component and the second invariant of velocity gradient tensor in the limit of incompressible flow. The structure of negative Reynolds stress component is similar to the coherent fine scale eddies.

Moreover, the far-field sound is predicted using acoustic analogies. By comparing the predicted far-field sound with the DNS result, Lighthill's and Powell's acoustic analogies are evaluated. For 4Λ source size, Lighthill's acoustic analogy can predict far-field sound excellently, while the amplitude of pressure fluctuation predicted by Powell's acoustic analogy shows significantly large values compared with the DNS result. For 3Λ source size, the pressure fluctuation predicted by Lighthill's acoustic analogy shows agreement with the DNS result until the period of vortex pairing, while it shows slightly small value compared with the DNS result after the mixing transition.

REFERENCES

Bastin, F., Lafon, P. and Candl, S., 1997, "Computation of jet mixing noise due to coherent structure: the plane jet case", *J. Fluid Mech.*, Vol. 335, pp. 261-304.

Colonius, T., Lele, S. K. and Moin, P., 1994, "The scattering of sound waves by a vortex-numerical simulations and analytical solutions", *J. Fluid Mech.*, Vol. 260, pp. 271-298.

Colonius, T., Lele, S. K. and Moin, P., 1997, "Sound generation in a mixing layer", *J. Fluid Mech.*, Vol. 330, pp. 375-409.

Crigthon, D. G., 1981, "Acoustics as a branch of fluid mechnichs", *J. Fluid Mech.*, Vol. 106, pp. 261-298.

Engquist, B. and Majda, A., 1979, "Radiation boundary conditions for acoustic and elastic wave calculations", *Comm. Pure and Appl. Math.*, Vol. 32, pp.313-357.

Ho, C. M. and Huerre, P., 1984, "Perturbed free shear layers", *Ann. Rev. Fluid Mech.*, Vol. 16, pp. 365-424.

Ho, C. M., Zohar, Y., Moser, R. D., Roger, M., Lele, S. K. and Buell, J. C., 1988, "Phase decorrelation streamwise vortices and acoustic radiation in mixing layers", *Proceedings of the summer program, CTR*, pp. 29-39

Howe, M. S., 1975, "Contributions to the theory of aerodynamics sound, with application to excess jet noise and the theory of the flute", *J. Fluid Mech.*, Vol. 71, pp. 625-673.

Huang, L. S. and Ho, C. M., 1990, "Small-scale transition in a plane mixing layer", *J. Fluid Mech.*, Vol. 210, pp. 475-500.

Laufer, J. and Yen, T. C., 1983, "Noise generation by a low-Mach-number jet", *J. Fluid Mech.*, Vol. 134, pp. 1-31.

Li Y., Tanahashi M. and Miyauchi T., 2000a, "Sound generation in compressible mixing layers", *Trans. Jpn. Soc. Mech. Eng., (in Japanese)*, Vol. 66, No. 646, B, pp. 1529-1534.

Li Y., Tanahashi M. and Miyauchi T., 2000b, "Sound generation in chemically reacting mixing layers", *Trans. Jpn. Soc. Mech. Eng., (in Japanese)*, Vol. 66, No. 648, B, pp. 2117-2124.

Lighthill M. J., 1952, "On sound generated aerodynamically: I. General theory", *Proc. R. Soc. Lond.*, Vol. A 211, pp. 564-587.

Lilley, G. M., 1994, "The radiated noise from isotropic turbulence", *Theoret. Comput. Fluid Dynamics*, Vol. 6, pp. 281-301.

Mitchell, B. E., Lele, S. K. and Moin, P., 1995, "Direct computation of the sound from a compressible co-rotating vortex pair, *J. Fluid Mech.*, Vol. 285, pp. 181-202.

Möhring, W., 1978, "On vortex sound at low Mach number", *J. Fluid Mech.*, Vol. 85, pp. 685-691.

Papamoschou, D. and Roshko, A., 1988, "The compressible turbulent shear layer: an experimental study", *J. Fluid Mech.*, Vol. 197, pp. 453-477.

Phillips, O. M., 1960, "On the generation of sound by supersonic turbulent shear layer", *J. Fluid Mech.*, Vol. 9, pp. 1-28.

Poinsot, T. and Lele, S. K., 1992, "Boundary conditions for direct simulation of compressible viscous flows, *J. Comput. Phys.*, Vol. 101, pp. 104-129.

Powell, A., 1964, "Theory of vortex sound", *J. Acoust. Soc. Am.*, Vol. 36, pp. 177-195.

Proudman, I., 1952, "The generation of noise by isotropic turbulence", *Proc. R. Soc. Lond.*, Vol. A214, pp. 119-132.

Tanahashi, M., Iwase, S. and Miyauchi, T., 2000, "Reynolds number dependence of turbulence structure in temporally developing turbulent mixing layers", *Fluids Engineering Conference of JSME*, (CD-ROM), Vol. 63.

Tanahashi, M., Iwase, S. and Miyauchi, T., 2001, "Appearance and Alignment with Strain Rate of Coherent Fine Scale Eddies in Turbulent Mixing Layer", *J. Turbulence*, Vol. 2:006.

Tanahashi, M. and Miyauchi, T., 1993, "Direct numerical simulation of chemically reacting mixing layers", *JSME Int. J. Series B*, Vol. 36, No. 2, pp. 307-312.

Tanahashi, M. Miyauchi, T. and Matsuoka, K., 1997a, "Coherent fine scale structure in temporally-developing turbulent mixing layer", *Turbulence, Heat and Mass Transfer*, Delft University Press, Vol. 2, pp. 461-470.

Tanahashi, M. Miyauchi, T. and Ikeda J., 1997b, "Scaling law of coherent fine scale structure in homogeneous isotropic turbulence", *Turbulence and Shear Flow Phenomena-1, First International Symposium*, Banerjee, S and Eaton, J. K. ed., pp. 59-64.